Experimental Study on Shear Stress-Displacement, Creep and Shear Slip Instability Behavior of Rock Fractures

Minglei Zhai (minglzcumt@126.com)
China University of Mining and Technology
Haibo Bai
China University of Mining and Technology

Research Article

Keywords: Rock fractures, Direct shear, Pre-peak tiered cyclic shear, Multistage loading shear creep, Failure mechanisms, Creep model

Posted Date: November 17th, 2021

DOI: https://doi.org/10.21203/rs.3.rs-1005997/v1

Abstract

Rock mass inherently contains discontinuities, and shear sliding of rock masses along discontinuities is the most common failure mode of rock mass in engineering practice (such as slope, dam and tunnel). In this study, the mechanical and failure properties of rock fractures were examined through direct shear tests, pre-peak tiered cyclic shear tests and multistage loading shear creep tests. The results show that the deformable memory of rocks can be observed from shear stress-shear displacement curves, namely reloading curves continued to increase along the loading curve of the last cycle under the pre-peak tiered cyclic shear loading. The envelopes of shear stress-shear displacement curves were similar to the variation trend of shear stress-shear displacement curves obtained in the direct shear test. Besides, the variation trend of residual shear displacement (RSD) and relative residual shear displacement (RRSD) before slip instability were obtained by the data analyses of rock mass under pre-peak tiered cyclic shear tests. It is found that the change in the friction and sliding state of rock fracture is the main reason for the fluctuation of shear stress-shear displacement curves. The Chen's method was used to process the multistage loading shear creep curves and the three creep stages were analyzed. Moreover, the complex creep models in some previous studies were discussed and the data of shear creep tests were successfully fitted to the classical Burgers model. This study provides a guidance for the study on the shear instability of rock fractures under different shear loading paths.

1. Introduction

Rock masses contain discontinuities inherently, such as faults, fractures, bedding planes and other planes of weakness [2; 5; 11; 15; 23]. For example, the Baihetan Hydropower Station, a very large construction project, indicated by field geological investigations that many discontinuities developed in the rock masses [4]. In the open-pit mine located to the west of Fushun City, China, the Cretaceous rock mass between reverse faults F_1 and F_{1A} was imposed a substantial impact by strong shear stresses, resulting in a large amount of fractured rock mass [16]. The shear strength of rock joints was lower compared with the intact rock materials, and shear failure of rock masses along pre-existing fractures was one of the most common failure modes in rock slopes, rock dams and tunnels [8]. Thus, it is important to understand and predict the shear behaviours of rock masses containing joints for the design and stability analysis of rock structures.

In recent years, great effort has been paid to investigate the mechanical features, energy evolution and morphology characteristics of rock fractures from various perspectives, e.g. complete shear stress-shear displacement curves, energy dissipation and absorption, and change regularity of surface roughness [1; 24; 25; 27]. Similar to intact coal sample easily influenced by confining pressure and external stress level, it is general accepted that influencing factors, such as shear load, applied shear stress level and cyclic shear stress may stronger affect the mechanics and failure properties of rock fractures (Meng et al., [7]. Due to the difficulty to obtaining natural rock fractures, the cement mortar fractures or rock fractures obtained by artificial splitting was mainly used to carry out relevant tests [26].

In terms of direct shear tests, Zhou et al. [26] prepared the irregular serrated structural planes with three different asperity heights made of cement mortar to perform direct shear tests to study the effect of structural plane to the slip burst, and the mechanism of in-situ slip burst was analyzed preliminarily. Afterwards, Meng et al. [6] carried out shear tests under constant normal loading (CNL) on tensile joints in three different types of rock, the test results indicated that the maximum AE hit rate of marble joints was attained before the peak shear stress when the normal stress was 1 MPa, and the AE hit rate became quiet during the ultimate sliding stage. Moreover, Meng et al. [10] carried out direct shear tests on split granite joints at various shear rates (0.001-0.1 mm/s) under different normal stresses, and the influences of the shear rate on the shear strength, post-peak shear behaviour and acoustic emission characteristics are analysed and discussed. Recently, Meng et al. [9] conducted direct shear tests under constant normal stress condition on artificial splitting cement mortar fractures and monitored the AEs during the shear failure process. Furthermore, rock fractures was usually subjected to tiered cyclic stress, such as s periodical change of the reservoir level and reciprocating motion of the train [19]. Thus, it is of considerable significance to study the impacts of tiered cyclic stress on the mechanical behaviours of rock fractures. Zhai et al. [20] conducted experiments on jointed marble specimens using servo-controlled testing machine to investigate the energy and deformation characteristics of rock joints under multi-stage shear loading-creep-unloading conditions. Additionally, to study the evolution characteristics of interface slip field under cyclic loading, a double shear model test study of granite specimen under constant confining pressure was designed and carried out by Yang et al. [17]. More recently, Zhai et al. [19] experimentally investigated rock samples with artificially prefabricated fractures by RDS-200 servocontrolled rock direct shear experimental apparatus, measured displacement characteristics and energy evolution under pre-peak tiered cyclic shear loading at a constant normal loading. And like intact coal and rocks, creep of discontinuities is also a part of the fundamental properties for rock fractures, which was prone to contribute to the large deformation of slope and surrounding rock of underground tunnel, or even landslide hazard [22], and delay failure may took place several days or years. Many scholars in this field have conducted large quantity of research work, and they have gained rich achievements. For example, Wang et al. [12] induced two types of fractures by means of modified shear and indirect tension and assembled the fractured rock samples following their initial formation and direct shear tests were performed under a constant normal force and stepwise increased shear creep loadings. Zhang et al. [21] conducted restrictive shear creep experiments to investigate the creep characteristics of key unit rocks in the slope potential slip surface and established creep models reflecting the creep-failure time and progressive-failure characteristics of rock. More recently, Wang et al. [13] investigated the three creep stages of shear creep tests in detail and proposed a method for predicting the accelerating creep stage, established an empirical creep model, and so on.

As illustrated by the above analysis, extensive research has been conducted on mechanical and failure features of the rock fractures by different authors. Nevertheless, minimal investigations exist which simultaneously deal with the shear stress-shear displacement, creep, and cyclic shear failure characteristics. Therefore, in this study, direct shear tests, pre-peak tiered cyclic shear tests and multistage loading shear creep tests are conducted on the rock fractures obtained by artificial

prefabrication method to study the shear failure characteristics and instability behaviour under various loading paths. The results of this study will contribute to the understanding of failure instability mechanism of rock fractures under different shear loading paths, and are of great significance for the prevention and control of slip instability hazards of rock mass with fractures in geotechnical engineering.

2. Materials And Methods

2.1. Sample preparation

The marble samples used in this test were collected from a quarry of Nanzhao county, Henan province, China. The results of apparatus testing showed that the main components of the marble were calcite, dolomite and magnesite. The marble sample was gray, with a particle size of 0.2-0.5 mm and a uniform texture. The cylindrical samples with a diameter of 50 mm and a height of 100 mm were machined according to ISRM (International Society for Rock Mechanics) requirements. The smoothness and flatness between the upper and lower surfaces were controlled within a tolerance of ±0.05 mm and ±0.02 mm, respectively (Fig. 1).

2.2. sample treatment

The intact marble sample was placed in the self-made splitting grinding tool to prepare rock fracture, as shown in Fig. 2(a). The tool was composed of upper and lower parts with the same shape and cylindrical grooves. Wedge-shape steel wire with the same arc degree was embedded in the middle of the groove and slightly protruded from the arc surface of the grooves. The section line in the middle of the rock sample coincided with the steel wire, guaranteeing the application of uniform linear compression stress on the side surface of the sample perpendicular to the axis. As shown in Fig. 2(b), under the action of the press machine, the formed fracture was parallel to the upper and lower ends of the sample, which was similar to the natural shape. Fig. 2(c) shows the simplified diagram of the rock sample with fractures.

2.3. Experimental device

The RDS-200 rock mechanics shear test system produced by the American GCTS company was used in this experiment. Fig. 3 shows the experimental instrument and the simplified diagram of test devices in this experimental system, respectively.

The normal and shear loading of the testing system are 100 kN and 50 kN controlled by an electro-hydraulic servo control system, and the displacement and loading accuracy are 10^{-3} mm and 10^{-4} MPa, respectively. This testing system has advantages of easy operation and simple programming process, as well as high reliability and accuracy. The whole testing system is composed of normal and shear mechanisms, including control cylinders, load sensor, displacement sensor, load conduction arm, pin, pressure head and base.

2.4. Testing scheme

Twelve samples with rock fractures were prepared in this experiment. To achieve a certain number of stages in the tiered loading experiment, six samples were used for the direct shear test to measure the shear strength of fractures, which provides a reference for the classification of shear stress in the tiered shear loading test. The normal stress was constant in the direct shear test and was set at 2.6, 5.2, 7.8, 10.4, 13.0 and 15.6 MPa, respectively. The shear direction was controlled by the shear rate at a speed of 0.5 mm/min and the shear displacement was 5 mm at the end of shear test.

The other two samples were used for the tiered cyclic shear test, and the normal stress was 1.5 MPa and 3.0 MPa, respectively. According to the average shear strength of the rock fractures and the enhanced damage effect of tiered cyclic loading on the fracture, the increment of cyclic shear stress was 0.4 MPa per cycle. The remained four samples were selected for the multistage shear creep test. The normal stress was constant and set as 1.5 MPa and 3.0 MPa. In the creep test, the force loading mode was adopted at a loading rate of 0.6 MPa/min. To provide sufficient creep deformation time for the samples, six stages of the stepped shear loading were set, and the stability of each stage lasted for 24 hours. Fig. 4 and Fig. 5 show the loading paths of multistage loading shear creep tests and tiered cyclic shear tests, respectively. The specific experimental procedures are shown in Table 1.

Table 1
Geometric information of samples with rock fracture and the experimental projects

Test type	Sample NO.	L (mm)	D (mm)	σ (MPa)
Direct shear	DS011	100.25	50.21	2.6
	DS012	100.16	49.85	5.2
	DS013	99.38	49.96	7.8
	DS014	99.86	50.06	10.4
	DS015	100.85	50.02	13.0
	DS016	100.08	50.07	15.6
Conventional multistage shear creep	CS151	100.32	49.91	1.5
	CS152	99.84	49.93	1.5
	CS301	100.26	50.02	3.0
	CS302	100.06	50.04	3.0
Tiered cyclic shear	TS151	99.82	50.02	1.5
	TS301	100.34	49.98	3.0

3. Experimental Results And Analysis

3.1 Complete shear stress-shear displacement curves

Figure 6 shows the complete shear stress-shear displacement curves of rock fractures under various normal stress. It can be seen that the shape of pre-peak curves of rock fractures under various normal stress are similar, while the shape of post-peak curves is different obviously. The pre-peak curves of rock fractures can be roughly divided into four stages: compaction stage, uniform rising stage, shear stress decline stage and residual strength stage. With the increase of the shear deformation, the shear stress increases rapidly. When the shear stress reaches the peak value, the shear resistance of rock fracture decreases significantly, and then irregular post-peak deformation or slipping phenomenon occurs.

In addition, the shear stress-shear displacement curves of rock fractures under the lower normal stress (e.g. σ = 2.6 MPa and 5.2 MPa) experiences a smoother decrease after the peak, and the slope shapes of the curves are concave; while the shear stress decreases sharply in an extremely short shear displacement or time under the higher normal stress (e.g. σ = 13.0 MPa and 15.6 MPa), resulting in a large gradient of descent. When the shear stress exceeds the peak shear strength, the shear failure occurs, and then slides along the fracture plane under the action of small shear stress. The small shear stress required to keep the sliding is the residual shear strength. The higher the normal stress, the higher the residual strength. As long as the normal stress exists, the shear fracture surface of rock still has the shear resistance.

During the shear process, there are many mechanical processes, such as elastic deformation of microbulges, splitting, generation and migration of particles, relative dislocation of rock fractures. As a result, the fluctuation in the residual shear strength curve is caused.

3.2 Tiered cyclic shear stress-shear displacement curves

3.2.1 Overall characteristics

Fig.7 shows the tiered cyclic shear stress-shear displacement curves of samples TS151 and TS301 at different cycle stages. As shown in Fig. 7, during the first cycle, the loading and unloading curves did not form a closed loop, and a large amount of residual shear displacement was observed. In a complete loading and unloading cycle, the loading curve did not coincide with the unloading curve, and the unloading curves were always lower than the loading curves due to the obvious plastic shear displacement of the rock fracture. The reloading shear stress-shear displacement curves continued to increase along the loading curve of the last cycle, indicating that the rock fractures had memory functions under prepeak tiered cyclic shear loading. The pre-peak tiered cyclic shear loading has little influence on the shear deformation behavior of rock fractures. The outer envelope of shear stress-shear displacement curves and direct shear curves have the same characteristics. Since the two samples have the similar shear displacement variations, the shear displacement change of rock fracture in the sample TS301 is described in detail (see Fig. 8). The envelope of shear stress-shear displacement curves can be roughly divided into four stages, that is, (□) compaction stage, (□) uniform rising stage, (□) shear stress decline stage and (□) friction sliding stage.

3.2.2 Residual shear displacement (RSD) and relative residual shear displacement (RRSD)

Residual shear displacement (RSD) is defined as the δ when the shear stress is unloaded to 0 MPa and RRSD is defined as the difference between the adjacent RSD (the RSD is equal to the RRSD during the first cycle). As presented in Fig. 7, the loading and unloading curves deviate far from each other during the first cycle. When the shear stress is unloaded to 0 MPa, a large RSD can be observed, which is mainly caused by the coupling compaction. Fig. 9 shows the RSD and RRSD of samples. It can be seen that the RSD increases linearly with the increase in the number of cycles. The RRSD is larger at the initial cycles and then decreases rapidly with the increase of cycles. Due to the existence of interspace between micro convexes of rock fractures, RRSD is relatively larger during the initial loading. With the increase of cycle numbers, RRSD decreases gradually and tends to be stable due to the extrusion action of the micro convex of rock fractures.

3.2.3 Shear slip during loading and unloading stages

As mentioned above, the loading and unloading curves of rock fracture in sample TS301 are described in Fig. 8. The shear stress-shear displacement curves of sample TS301 in loading and unloading stages are shown in Fig. 10(a) and (b), respectively. It can be seen that the morphological characteristics of shear stress-shear displacement curves are similar in the loading or unloading stage. and the curves can be roughly divided into two sections with the slip position as the boundary. At the slip position, the smaller change of shear stress leads to larger shear displacement, which was called shear slip, but this shear slip dose not lead to shear instability failure of rock fractures. For instance, in the forth curve in the unloading stage, shear displacement decreases significantly (0.859 - 0.753 mm), while the shear stress decreases slightly (0.29 - 0.22 MPa). The shear stress at the place of the slip occurrence is basically maintained within a certain range, and the shear stress does not change with the cycle progression. When sliding occurs in the shear loading, the shear stress of the TS301 sample is about 0.43 - 0.46 MPa; when the sliding occurs in the shear unloading, that of the TS301 sample is about 0.22 - 0.29 MPa. The rapid increase of shear displacement in the loading or unloading stage is different from the shear slip instability caused by the loading of the last cycle. The increasing shear stress can be sustained by fracture after a short slip, whereas the large displacement can be caused in the last stage, resulting in a high possibility of serious damage in engineering practice.

The underlying reasons for the fluctuation in curves can be explained from the angle of friction state changes. When the shear stress was lower, the coupling fractures are in the state of static friction, and shear displacement is mainly caused by the rock fracture; there is a small elastic displacement of the randomly distributed bump and convex body, indicating the great compaction of coupling fracture. At this time, wear particles in the fracture were caused by the increasing shear displacement, and the number of particles increased with the increase of shear stress. With the increase of shear stress, the fracture is in the state of static friction and sliding friction alternately. However, the effect of static friction on the fracture surface was weakened by wear particles, and the overall sliding rate increases rapidly. With the

increase of the shear stress, shear stress-shear displacement curves present a nearly linear increasing trend, and static friction is changed into sliding friction. Then the influence of wear particles on shear displacements and shear slip rates of convexes was weakened. Therefore, the change of friction state of the rock fractures is the main cause of the fluctuation of shear stress-shear displacement curves.

3.3 Creep curves

Figure 11 and Fig. 12 show the original creep curves and the curves obtained by Chen's method. The shear displacement of rock fracture is also sensitive to stress (e.g. normal or shear stress) and time (such as creep and relaxation) [22]. In general, the idealized shear creep curve of rock fracture usually exhibits four principal phases, which are the same as the uniaxial and triaxial creep curve of intact rock and coal [22]: (1) instantaneous shear displacement because of instantaneous shear stress; (2) primary creep stage with sharp displacement increments, but at a decelerated displacement rate; (3) steady-state creep stage at low, or near-constant displacement rate; (4) accelerated creep stage with rapid displacement increment until failure occurs, or failure during shear stress application.

Similar to the coal sample, it was almost unrealistic for all rock fracture samples to achieve the ideal accelerated creep through prejudging the shear stress and the time given for the rock fracture to creep. As shown in Fig. 12, the sample CS152 does not experience the ideal tertiary creep in the timescale. In the final loading process, the shear stress first rises sharply to the maximum value, and then suddenly decreases, indicating the occurrence of the failure phenomenon. The samples CS151, CS301 and CS302 all reach the ideal accelerated creep. Considering that the accelerated creep curves of the three samples are similar, only the sample CS301 is analyzed.

Generally speaking, when the rock fracture is subjected to instantaneous shear stress, the shear displacement shows a jump, e.g. the AB stage in Fig. 13. When the imposed shear stress was constant, the primary creep occurs at a decelerating displacement rate, i.e. BC segment, and point B is the initiating point of creep. The steady-state creep is apparent (CD curve) as time goes on. Then the sample is gradually transformed from steady-state creep to accelerated creep (DE curve).

3.4 Analysis of creep model

Based on shear creep curves obtained by Chen's method in Fig. 12, it can be seen that the marble fractures obtained by the artificial prefabrication method have distinct visco-elastic behavior at various shear stress levels. To describe visco-elastic shear creep behavior of rock fractures, the Hookean body and Newton body are usually connected in series or parallel to form all kinds of visco-elastic creep models, such as the Maxwell model, Kelvin model.

Complex creep models have been used to fit the creep curves under different stress states in previous studies, and the determined model parameters irregularly change with the stress state. The suitability of the model can only be judged according to the fitting accuracy of the curve. It should be emphasized that if multiple parameters in the fitting formula are determined only for a set of data or a curve, the formula

can certainly be in good agreement with the set of data or curve, but the correctness and rationality of the formula cannot be proved, or the formula can not be applied to any other occasions.

To refer to such a formula as a "mechanical model or theory" is to misunderstand the meaning of "model" and "theory". However, choosing complex formulas and too many undetermined parameters to pursue too high fitting accuracy may completely distort the variation law of parameters expressed by fitting formulas [18]. In this research, the traditional Burgers model was chosen to study the visco-elastic shear creep behavior of rock fractures (see Fig. 14).

The creep equation of Burgers model under the action of constants shear stress is

$$u_{creep}(t)=\frac{\tau}{G_M}+\frac{\tau}{\eta_M}t+\frac{\tau}{G_K}\left(1-\exp\left(-\frac{G_K}{\eta_K}t\right)\right) \tag{1}$$

where $u_{creep}(t)$ is the shear displacement measured at a certain time t; E_M and η_M are Kelvin's shear modulus and viscosity coefficient; E_M and η_M are the Maxwell's shear modulus and viscosity coefficient, respectively.

On the basis of shear creep test curves, the regression inversion method was used to identify the parameters based on the 1stopt fitting software. In the identification, one of the squares of correlation coefficient (R^2) is regarded as the discrimination criterion [14]. It needs to be noted that R^2 tends to 1.0, which means that the theoretical model agrees better with the experimental data. In accordance with Fig. 15 and Eq. (1), the creep parameters for the Burgers model at each creep stage can be identified. Fig. 15 shows the comparison between the predicted curve by the Burgers creep model and experimental result under different shear stress, and the fitting results are listed in Table 2. As shown in Fig. 15, it can be seen that the Burgers creep model has a good agreement with experimental results.

Table 2
Shear creep model parameters of rock fractures with various shear stress levels.

	τ (MPa)	G_M (MPa·mm)	η_M (MPa·h/mm)	G_K (MPa·mm)	η_K (MPa·h/mm)	R^2
CS151						
Stage1	1.0	1.383	483.714	300.230	588.089	0.884
Stage2	1.4	1.624	717.469	315.171	1.588	0.869
Stage3	1.8	1.781	481.482	0.761	376.228	0.797
Stage4	2.2	1.988	111.559	1.206	310.153	0.999
CS152						
Stage1	1.0	1.942	781.358	56.927	165.396	0.892
Stage2	1.4	2.128	1416.252	24.997	327.410	0.865
Stage3	1.8	2.304	1470.839	174.445	384.159	0.822
Stage4	2.2	—	—	—	—	—
CS301						
Stage1	2.0	1.524	919.841	69.752	134.302	0.989
Stage2	2.4	1.645	2943.517	118.437	249.400	0.975
Stage3	2.8	1.799	2132.474	217.088	250.829	0.971
Stage4	3.2	1.923	4529.709	176.406	482.765	0.959
Stage5	3.6	2.063	5158.879	330.209	680.983	0.874
Stage6	4.0	2.192	1251.067	102.053	100.517	0.966
CS302						
Stage1	2.0	2.018	1310.915	182.299	23329	0.969
Stage2	2.4	2.160	1501.632	165.269	4.812	0.964
Stage3	2.8	2.284	4462.384	178.421	476.329	0.929
Stage4	3.2	2.429	3917.103	116.276	192.894	0.952
Stage5	3.6	2.532	3889.150	352.215	146.1	0.923
Stage6	4.0	2.678	3844.134	224.830	13.898	0.991

4. Conclusions

The main goal of this study is to investigate the shear failure characteristics and instability behaviour of rock fractures obtained by artificial prefabrication method under various loading paths (including direct shear, pre-peak tiered cyclic shear and multistage loading shear creep simultaneously). The operations mainly consisted of three series of tests (listed in Table 1) where normal stress was held constant in each project. Based on these analysis, the following conclusions are drawn:

(1) The shape of pre-peak shear stress-shear displacement curves of rock fractures are similar under various normal stress. These curves can be divided into compaction stage and uniform rising stage. However, the post-peak curves are different significantly and irregular post-peak deformation or slip phenomenon occurs. The shape of these curves is concave after the post-peak shear stress under the lower normal stress; while the shear stress decreases sharply within an extremely short shear displacement or time under higher normal stress. Regardless of direct shear, pre-peak tiered cyclic shear or multistage loading shear creep, all rock fractures show transient failure features after peak shear stress in the shear stress-shear displacement curves.

(2) The deformable memory of rocks can be observed from shear stress-shear displacement curves, that is, the reloading curves continue to increase along the loading curves of the last cycle under pre-peak tiered cyclic shear loading. The pre-peak tiered cyclic shear loading has little effect on the shear deformation behavior of rock fracture, and the outer envelopes of shear stress-shear displacement curves are similar to those obtained in the direct shear test, and the envelope lines of pre-peak tiered cyclic shear stress-shear displacement curves can also be divided into compaction stage, uniform rising stage, shear stress decline stage and friction sliding stage. Generally, the RSD and RRSD are affected by cyclic numbers; with the increasing number of cycles, the RSD increases and the RRSD decreases.

(3) When the shear stress is loaded or unloaded to a certain stress level, the shear displacement increases or decreases rapidly, while the sudden instability of the rock fracture will not occur. The shear slip is caused by the transformation of static friction, and the fluctuation of shear stress-shear displacement curves is mainly caused by the sliding friction and the change of friction and sliding state of rock fracture.

(4) The data of shear creep tests are successfully fitted to the Burgers model, exhibiting visco-elastic characteristics. The fitting results show that G_M is far less than that of other shear creep parameters. However, η_M is much larger than other shear creep parameters and can be used to reflect the variation of the shear displacement rate of the secondary creep; η_M linearly increases with the rise in shear stress. On the contrary, with the increase of shear stress, both elastic shear displacement and viscous flow increase, G_K and η_K have the randomness and volatility.

The range of shear stress level applied to the rock fractures, and the timescale applied to the investigation of creep might somewhat limit the findings. Therefore, future work may be conducted using different types of rock fractures to study its mechanical features, and with a broader range of normal and shear stress, as well as enough time given to the rock fractures to shear creep. Nevertheless, these

findings in the present paper provide a theoretical framework for future studies to assess the geomechanics and failure mechanisms of rock fractures.

Declarations

Acknowledgments

This work was supported by the National Natural Science Foundation of China (50974115). We would like to express our gratitude to all those who have helped us during the writing of this paper. We gratefully acknowledge the help from Professor Baohua Guo at HPU. We would like to thank ShiningStar Translation for providing linguistic assistance during the preparation of this manuscript.

References

1. Ge, Y. F. et al. Strain Energy Evolution of Penetrative Rock Joints Under Shear Loading. *Chinese Journal of Rock Mechanics and Engineering*. 35, 1111-1121 (2016).
2. Ge, Y. F. et al. Determination of Shear Failure Regions of Rock Joints Based On Point Clouds and Image Segmentation. *ENG GEOL*. 260, 105250 (2019).
3. Guo, B. H. & Dong, H. Y. Shear Failure Modes and AE Characteristics of Sandstone and Marble Fractures. *OPEN GEOSCI*. 11, 249-262 (2019).
4. Jia, C. J., Xu, W. Y., Wang, R. B., Wang, S. S. & Lin, Z. N. Experimental Investigation On Shear Creep Properties of Undisturbed Rock Discontinuity in Baihetan Hydropower Station. *INT J ROCK MECH MIN*. 104, 27-33 (2018).
5. Kou, M. M., Liu, X. R., Tang, S. D. & Wang, Y. T. Experimental Study of the Prepeak Cyclic Shear Mechanical Behaviors of Artificial Rock Joints with Multiscale Asperities. *SOIL DYN EARTHQ ENG*. 120, 58-74 (2019).
6. Meng, F. Z. et al. Shear Behaviour and Acoustic Emission Characteristics of Different Joints Under Various Stress Levels. *ROCK MECH ROCK ENG*. 49, 4919-4928 (2016).
7. Meng, F. Z. et al. Experimental Study of Factors Affecting Fault Slip Rockbursts in Deeply Buried Hard Rock Tunnels. *B ENG GEOL ENVIRON*. 76, 1167-1182 (2017).
8. Meng, F. Z., Wong, L. N. Y., Zhou, H. & Q, W. Z. Comparative Study On Dynamic Shear Behavior and Failure Mechanism of Two Types of Granite Joint. *ENG GEOL*. 356-369 (2018).
9. Meng, F. Z., Wong, L. N. Y., Zhou, H., Wang, Z. Q. & Zhang, L. M. Asperity Degradation Characteristics of Soft Rock-Like Fractures Under Shearing Based On Acoustic Emission Monitoring. *ENG GEOL*. 266, 105392 (2020).
10. Meng, F. Z., Wong, L. N. Y., Zhou, H., Yu, J. & Cheng, G. T. Shear Rate Effects on the Post-Peak Shear Behaviour and Acoustic Emission Characteristics of Artificially Split Granite Joints. *ROCK MECH ROCK ENG*. 52, 2155-2174 (2019).

11. Shen, M. R. & Zhang, Q. Z. Study of Shear Creep Characteristics of Greenschist Discontinuties. *Chinese Journal of Rock Mechanics and Engineering*. 29, 1149-1155 (2010).
12. Wang, J. A., Wang, Y. X., Cao, Q. J., Ju, Y. & Mao, L. T. Behavior of Microcontacts in Rock Joints Under Direct Shear Creep Loading. *INT J ROCK MECH MIN*. 78, 217-229 (2015).
13. Wang, Z., Gu, L. L., Zhang, Q. Z., Yue, S. L. & Zhang, G. K. Creep Characteristics and Prediction of Creep Failure of Rock Discontinuities Under Shearing Conditions. *INT J EARTH SCI*. 109, 945-958 (2020).
14. Yang, S. Q. & Cheng, L. Non-Stationary and Nonlinear Visco-Elastic Shear Creep Model for Shale. *INT J ROCK MECH MIN*. 48, 1011-1020 (2011).
15. Yang, S. Q. & Ni, H. M. A Viscoelastic Shear Creep Model of Mudstone Parameter Identification. *Journal of China Univercity of Mining and Technology*. 41, 551-557 (2012).
16. Yang, T. H. et al. Rheological Characteristics of Weak Rock Mass and Effects on the Long-Term Stability of Slopes. *ROCK MECH ROCK ENG*. 47, 2253-2263 (2014).
17. Yang, X. B., Zhou, J., Song, Y. M. & Han, X. X. Evolution Characteristics of Sliding Displacement of Rock Interface Under Cyclic Loading. *Journal of China Coal Society*. 44, 3041-3048 (2019).
18. You, M. Q. Discussion On Mathematical Fitness and Mechanical Model of Experimental Results. *Chinese Journal of Rock Mechanics and Engineering*. 27, 251-257 (2008).
19. Zhai, M. L., Bai, H. B. & Wu, L. Y. Shear Slip Instability Behavior of Rock Fractures under Prepeak Tiered Cyclic Shear Loading. *ADV CIV ENG*. 2020, 1-12 (2020).
20. Zhai, M. L., Guo, B. H., LI, B. Y. & Jiao, F. Energy and Deformation Characteristics of Rock Joints Under Multi-Stage Shear Loading-Creep-Unloading Conditions. *Rock and Soil Mechanics*. 39, 2865-2872 (2018).
21. Zhang, H. et al. Creep Characteristics and Model of Key Unit Rock in Slope Potential Slip Surface., 2019:4019094.
22. Zhang, L., Li, X. C. & Ren, T. A Theoretical and Experimental Study of Stress–Strain, Creep and Failure Mechanisms of Intact Coal. *ROCK MECH ROCK ENG*. 53, 5641-5658 (2020).
23. Zhang, Q. Z., Shen, M. R. & Ding, W. Q. Study On the Shear Creep Characteristics and Constitutive Model of Rock Mass Discontinuity. *China Civil Engineering Journal*. 44, 127-132 (2011).
24. Zhang, Q. Z., Shen, M. R. & Ding, W. Q. Study of Shear Creep Constitutive Model of Greenschist Structural Plane. *Rock and Soil Mechanics*. 33, 3632-3638 (2012).
25. Zhang, Z. L., Xu, W. Y., Zhao, H. B. & Jian, B. Investigation On Shear Creep Experiments of Sandstone with Weak Plane in Xiangjiaba Hydropower Station. *Chinese Journal of Rock Mechanics and Engineering*. 29, 3693-3698 (2010).
26. Zhou, H., Meng, F. Z., Zhang, C. Q., Yang, F. J. & Lu, J. J. Characteristics of Shear Failure of Structural Plane and Ship Rockburst. *Chinese Journal of Rock Mechanics and Engineering*. 34, 1729-1738 (2015).

27. Zhu, S. N., Yin, Y. P., Li, B. & Wei, Y. J. Shear Creep Characteristics of Weak Carbonaceous Shale in Thick Layered Permian Limestone, Southwestern China. *J EARTH SYST SCI*. 128, (2019).

Figures

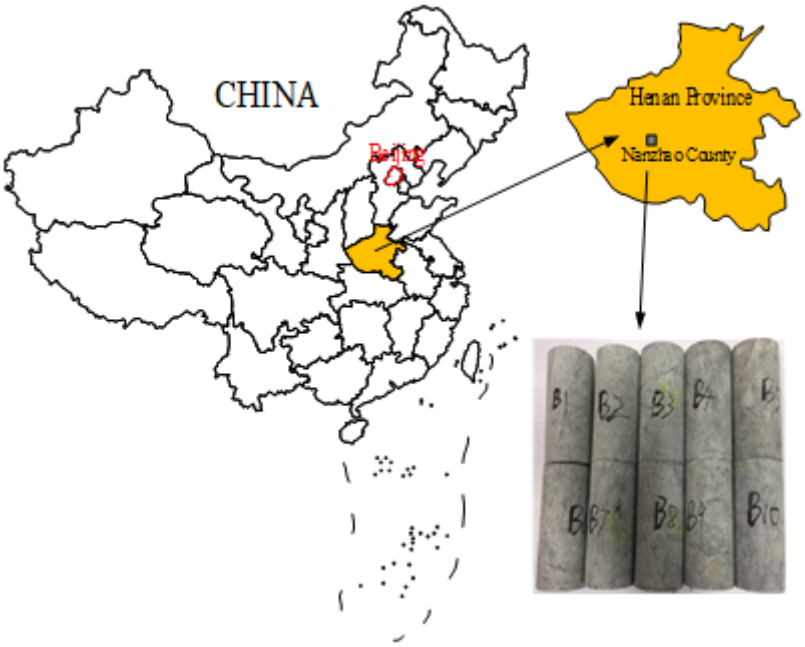

Figure 1

Sampling location and some rock samples

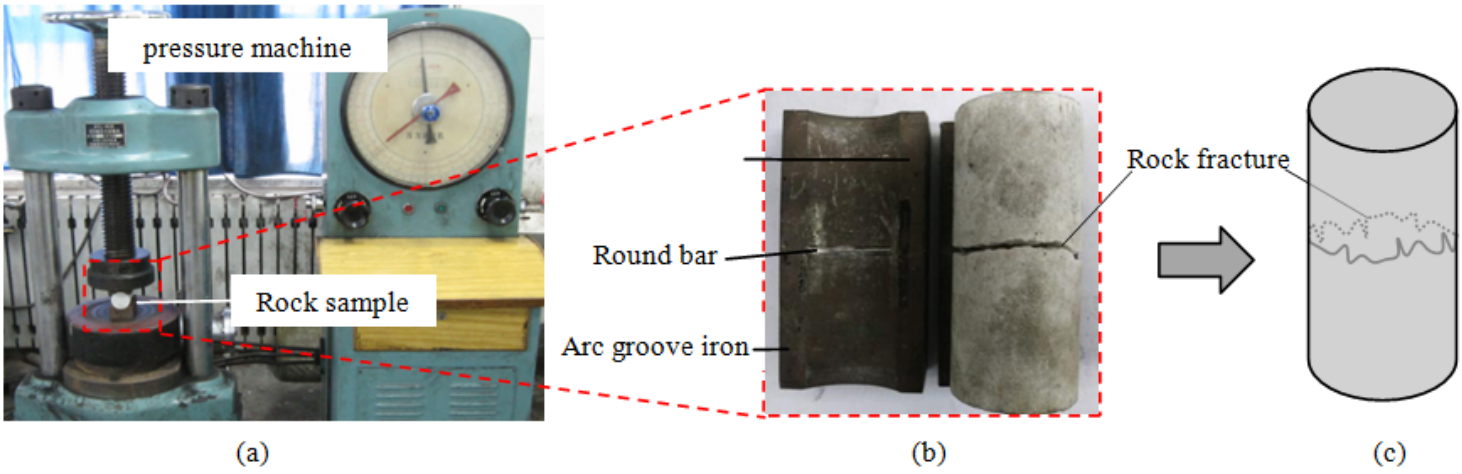

Figure 2

Specimen processing: (a) the manufacture of rock fracture. (b) rock fracture and splitting tool. (c) simplified diagram.

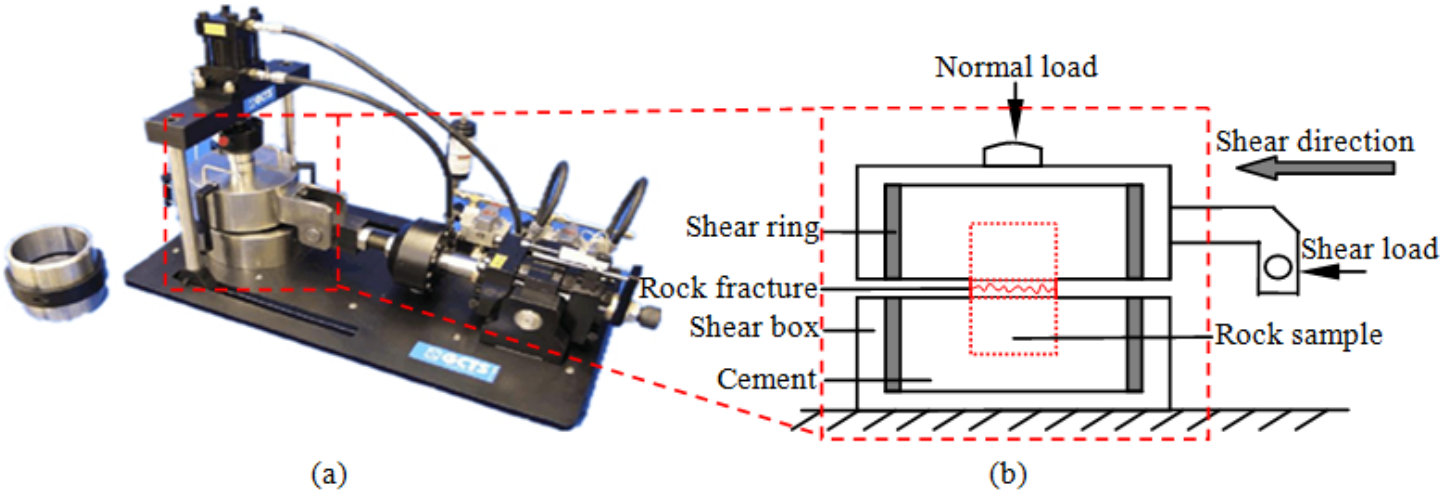

Figure 3

Test equipment and simplified diagram: (a) shear test system. (b) simplified diagram of the testing system [3].

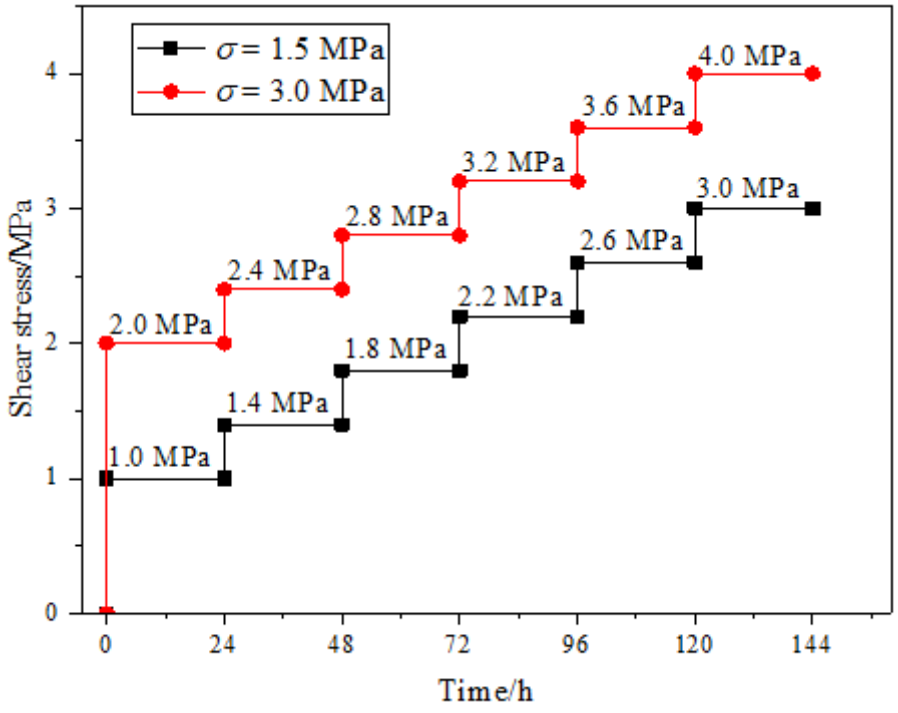

Figure 4

Shear stress paths of multi-step creep tests

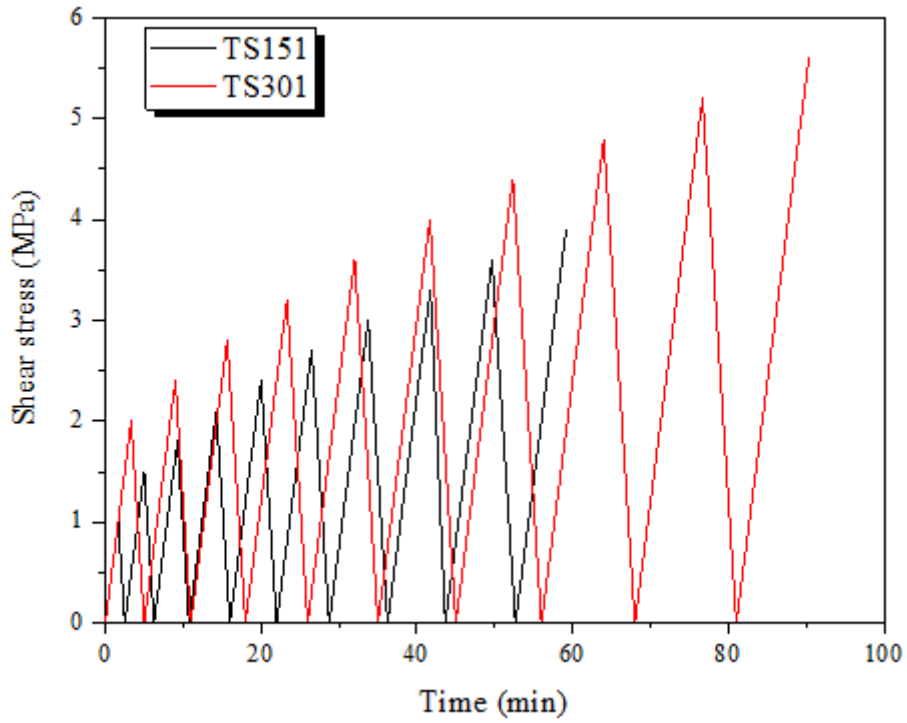

Figure 5

The tiered loading-unloading cycles for shear testing

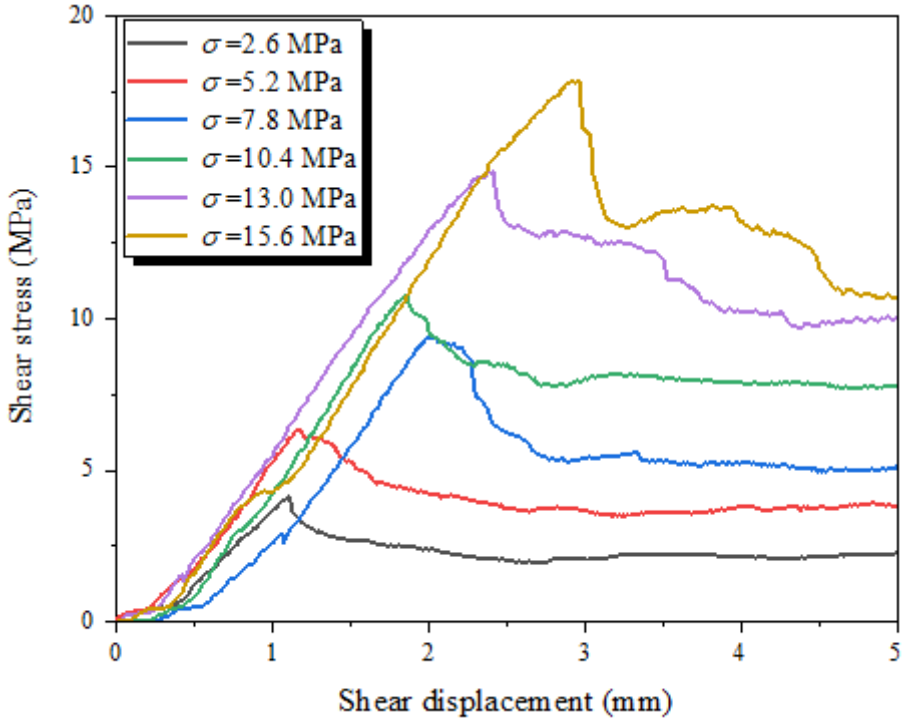

Figure 6

Shear stress-shear displacement curves of marble fractures

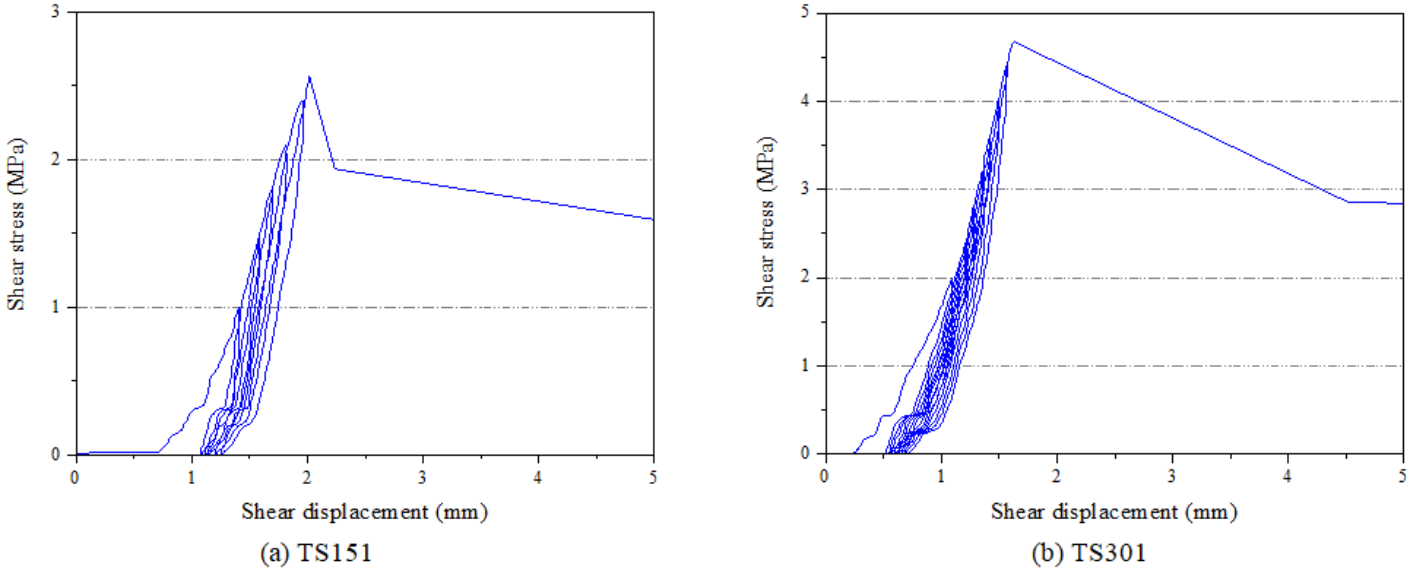

Figure 7

Tiered cyclic shear stress-shear displacement curves

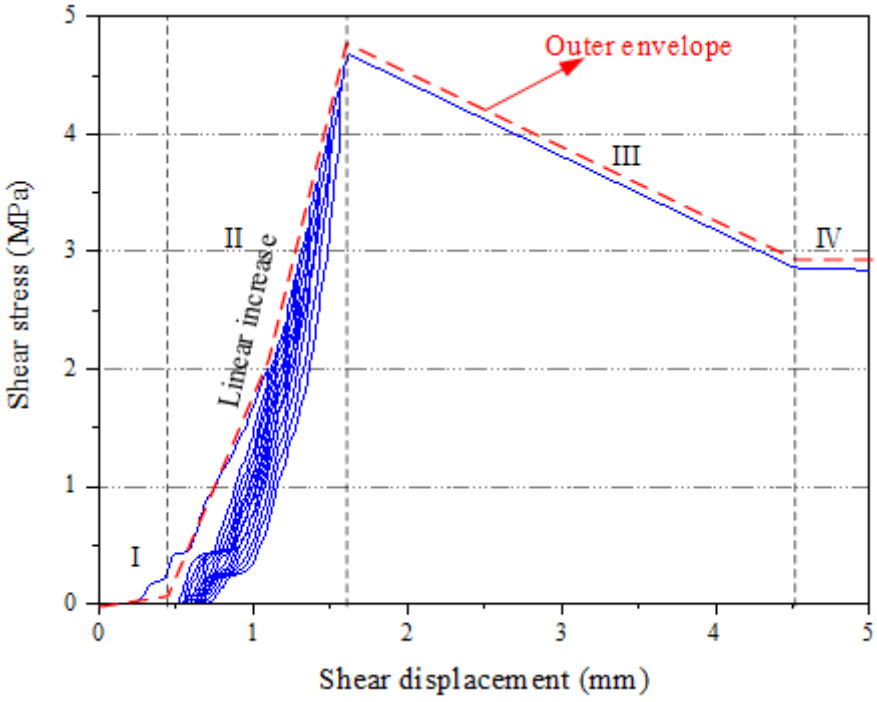

Figure 8

The four stages of overall curves

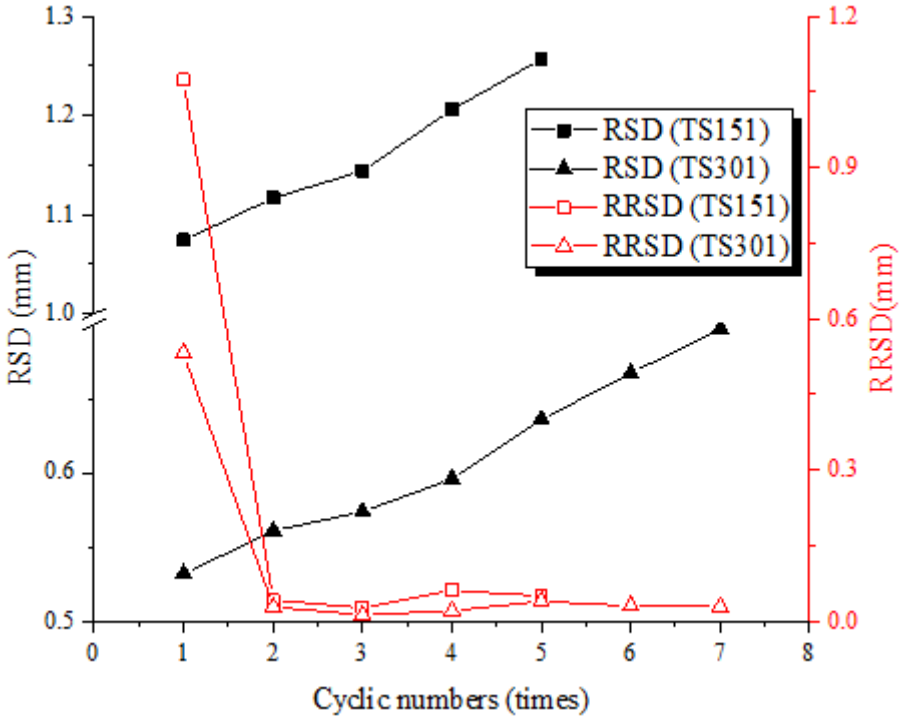

Figure 9

RSD and RRSD in different cyclic numbers

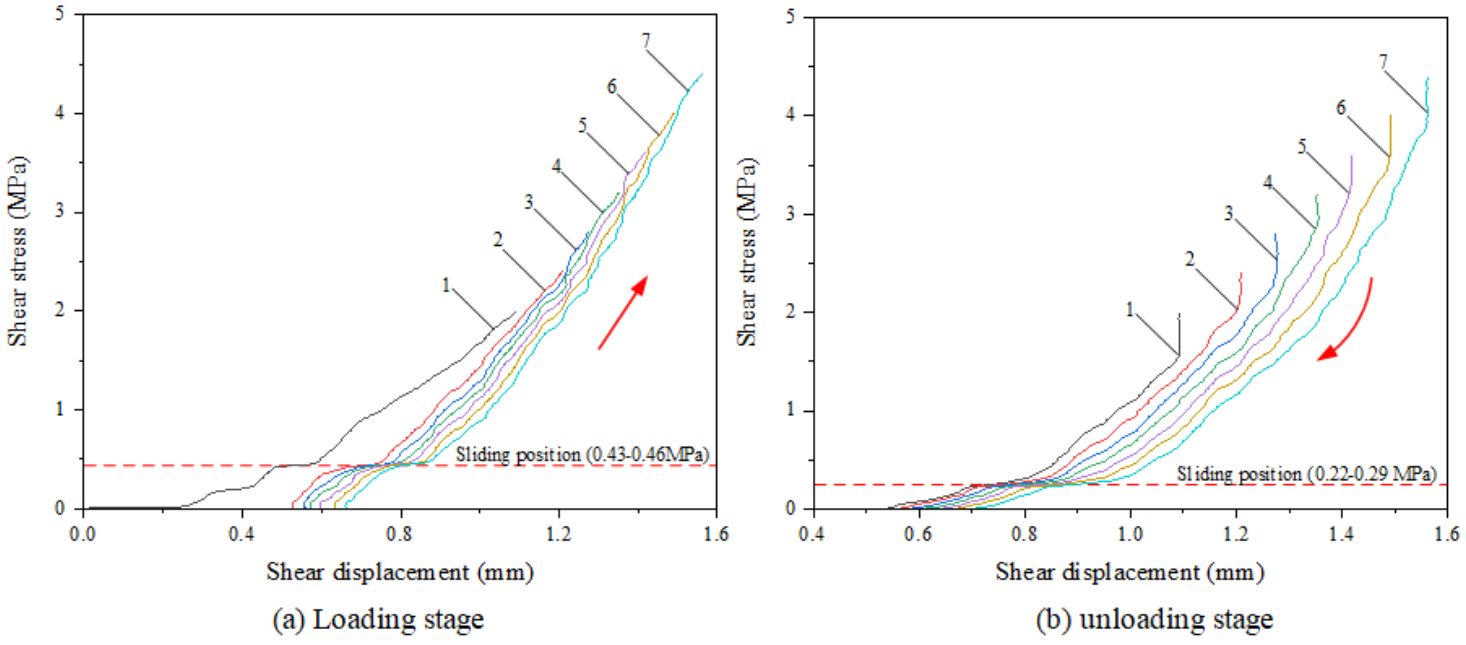

Figure 10

Sliding position and loading and unloading curves of sample TS301

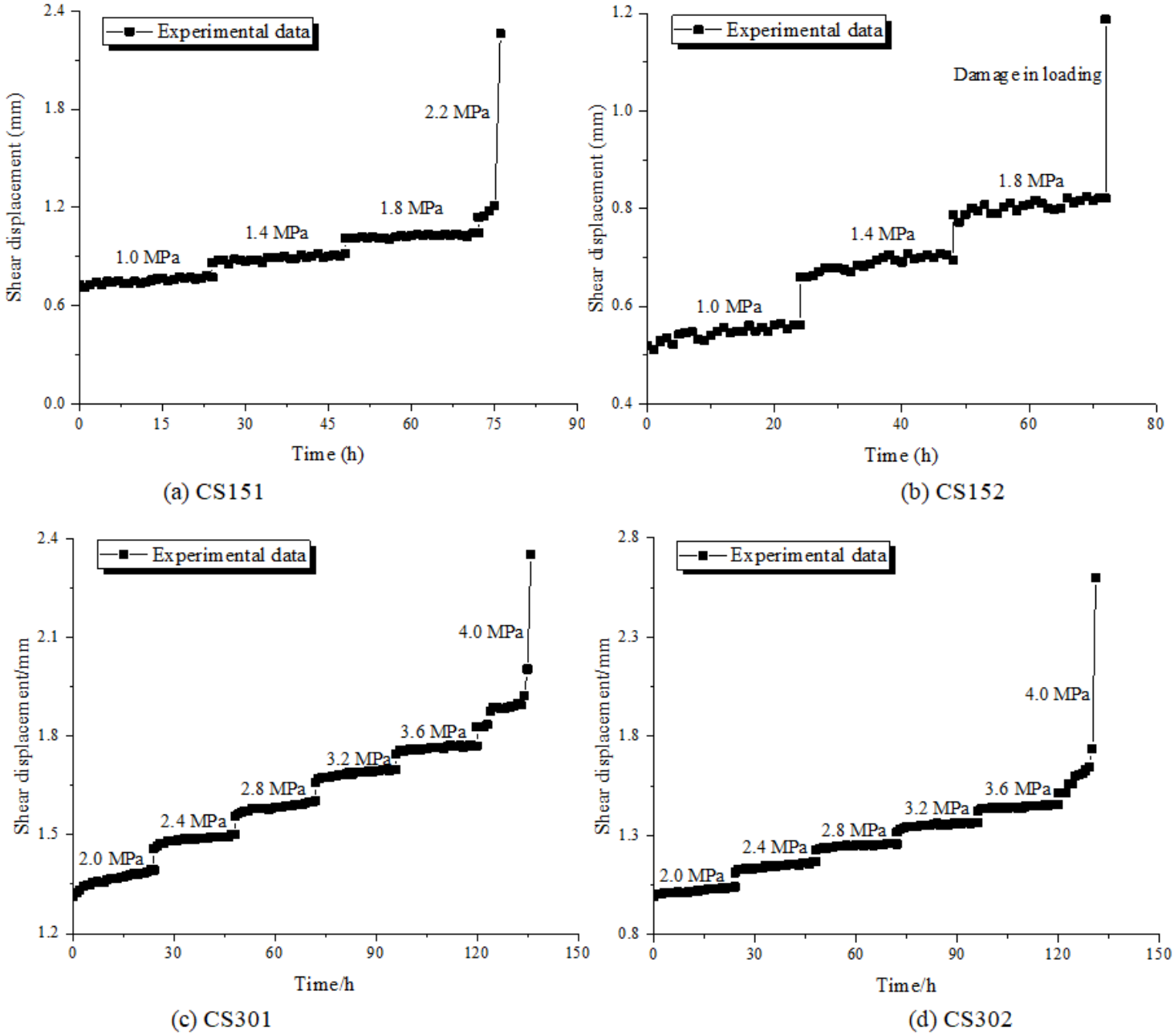

Figure 11

The original creep curves

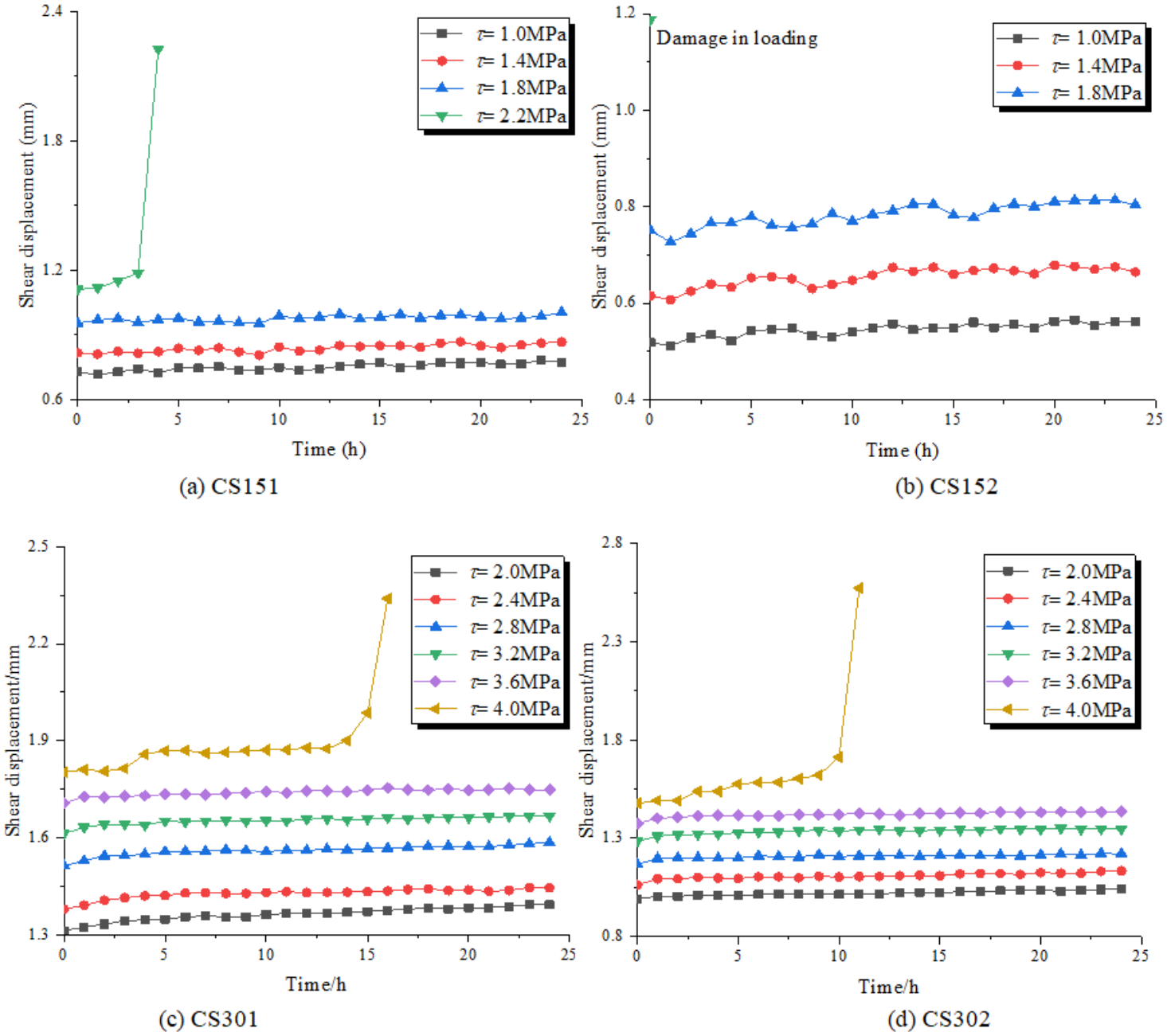

Figure 12

the curves treated by Chen's method

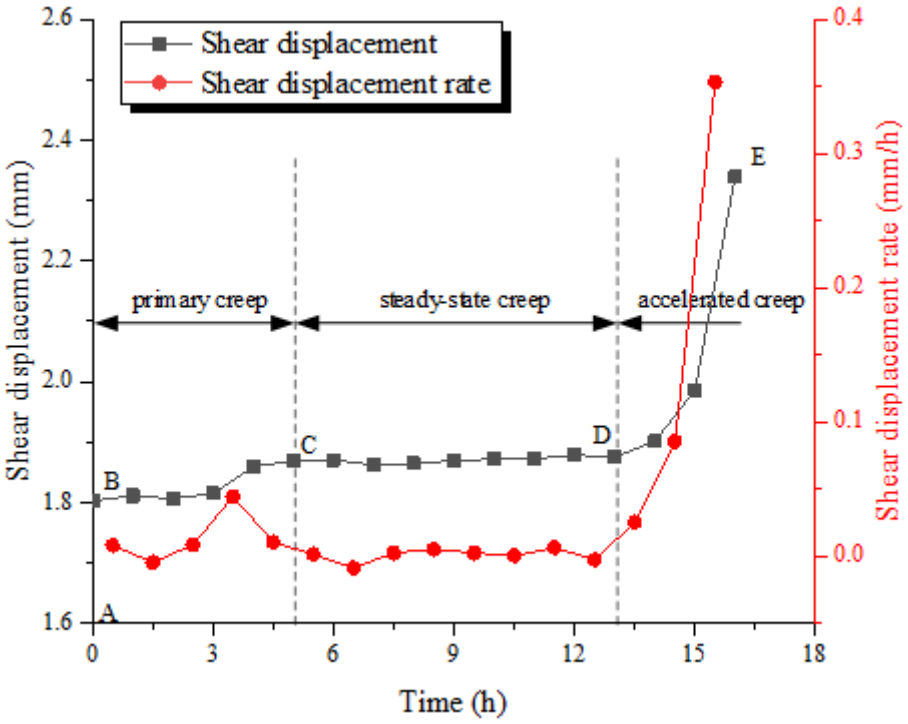

Figure 13

Typical curve of shear creep. Taking the sample CS301 under shear stress (τ=4.0 MPa) as an example.

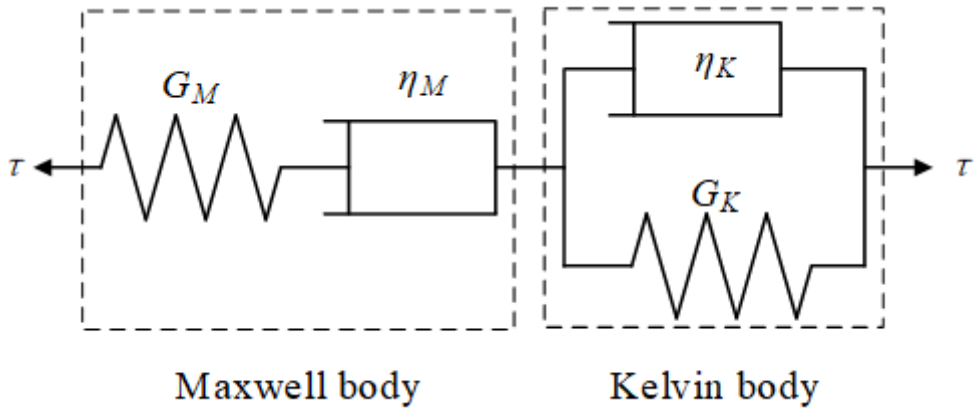

Figure 14

Burgers model

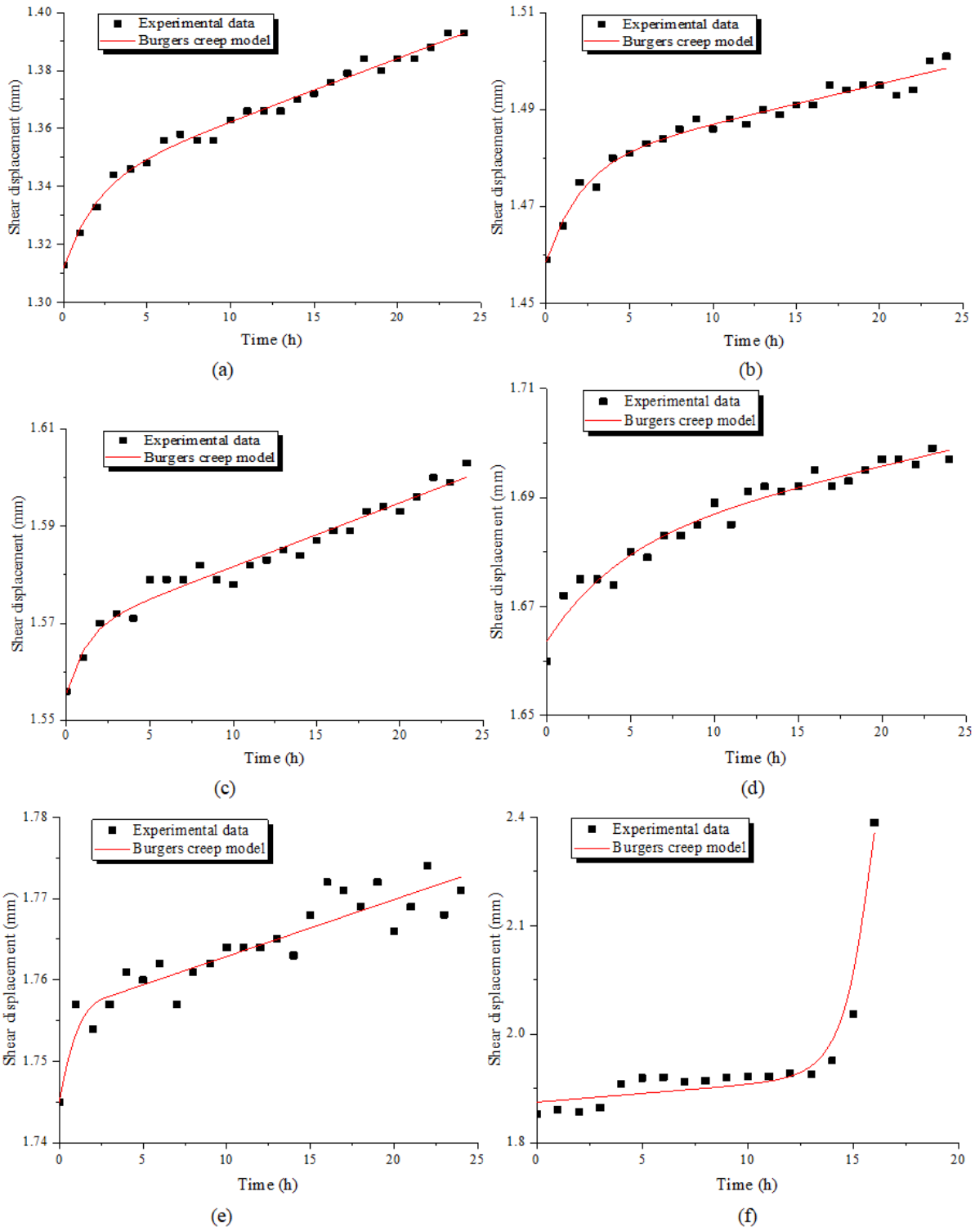

Figure 15

Comparison between predicted curve by Burgers creep model and experimental result under different shear stress: (a) 2.0 MPa, (b) 2.4 MPa, (c) 2.8 MPa, (d) 3.2 MPa, (e) 3.6 MPa, (f) 4.0 MPa.